et al. Clinical practice guidelines for the management of candidiasis: 2009 update by the Infectious Diseases Society of America. *Clin Infect Dis* 2009;48:503–535.
16. Limper AH, Knox KS, Sarosi GA, Ampel NM, Bennett JE, Catanzaro A, Davies SF, Dismukes WE, Hage CA, Marr KA, *et al*. An official American Thoracic Society statement: treatment of fungal infections in adult pulmonary and critical care patients. *Am J Respir Crit Care Med* 2011;183:96–128.
17. Emanuel EJ, Thompson DF. The concept of conflicts of interest. In: Emanuel EJ, Grady C, Crouch RA, Lie RK, Miller FG, Wendler D, editors. The Oxford textbook of clinical research ethics. New York: Oxford University Press; 2008. pp. 758–766.
18. Hampson LA, Bekelman JE, Gross CP. Empirical data on conflicts of interest. In: Emanuel EJ, Grady C, Crouch RA, Lie RK, Miller FG, Wendler D, editors. The Oxford textbook of clinical research ethics. New York: Oxford University Press; 2008. pp. 767–779.
19. Angell M. Industry-sponsored clinical research: a broken system. *JAMA* 2008;300:1069–1071.
20. Weinberger SE. Providing high-value, cost-conscious care: a critical seventh general competency for physicians. *Ann Intern Med* 2011;155:386–388.
21. Rosenbaum L, Lamas D. Cents and sensitivity: teaching physicians to think about costs. *N Engl J Med* 2012;367:99–101.
22. Horwitz E, Shavit O, Shouval R, Hoffman A, Shapiro M, Moses AE. Evaluating real-life clinical and economical burden of amphotericin-B deoxycholate adverse reactions. *Int J Clin Pharm* 2012.
23. Imhof A, Walter RB, Schaffner A. Continuous infusion of escalated doses of amphotericin B deoxycholate: an open-label observational study. *Clin Infect Dis* 2003;36:943–951.

Exonic Mutations of *TSC2/TSC1* Are Common but Not Seen in All Sporadic Pulmonary Lymphangioleiomyomatosis

To the Editor:

Pulmonary lymphangioleiomyomatosis (LAM) is a rare, progressive disease affecting almost exclusively women that is seen in both patients with tuberous sclerosis complex (TSC) and those without TSC, the latter termed sporadic LAM (S-LAM) (1–5). LAM is characterized by infiltration of the lung parenchyma by neoplastic spindle-shaped cells with combined smooth muscle and melanocytic differentiation, and is associated with both extensive involvement of lymphatic channels by similar cells in nearly all cases, and occurrence of renal angiomyolipoma in 30 to 50% of S-LAM cases (3). Past seminal publications identified mutations and loss of heterozygosity (LOH) in *TSC2* in pulmonary LAM cells of four S-LAM patients who had angiomyolipomas with known mutations (6), and in two of five S-LAM patients (7). Other studies have shown that *TSC2* mutations are seen in cultured LAM cells (8), and that *TSC2* LOH is seen in LAM cells isolated from blood, urine, chylous fluid, and bronchoalveolar lavage fluid in 50 to 90% of S-LAM patients (9, 10). Some of the results of this study have been previously reported in the form of abstracts (11, 12).

We searched for *TSC2* mutations in 10 S-LAM patients that had lung transplant using a combination of laser capture microdissection (LCM) and next-generation sequencing (NGS) (*see* online supplement). Examination of formalin-fixed paraffin-embedded sections showed classic features of LAM, with multiple cysts and disseminated LAM nodules, the cells of which were smooth muscle actin (SMA) and HMB45 positive (Figures E8A–E8G in the online supplement). LCM guided by SMA immunohistochemistry was performed on frozen sections to collect LAM cells from nodules (Figure E1) and avoid inclusion of lymphatic channels, lymphocytes, and other cell types (Figures E3 and E4). After DNA extraction and amplification, NGS was performed using either the 454 or Illumina platforms (Reference 13 and online supplement). High read depth was achieved across the coding region of *TSC2* (median, 486; >200 in 96% of exons), enabling detection of low-frequency sequence variants. Nine different pathogenic sequence variants were detected in *TSC2* in eight different sporadic LAM samples, at frequencies ranging from 4 to 60% (Table 1), with most seen at

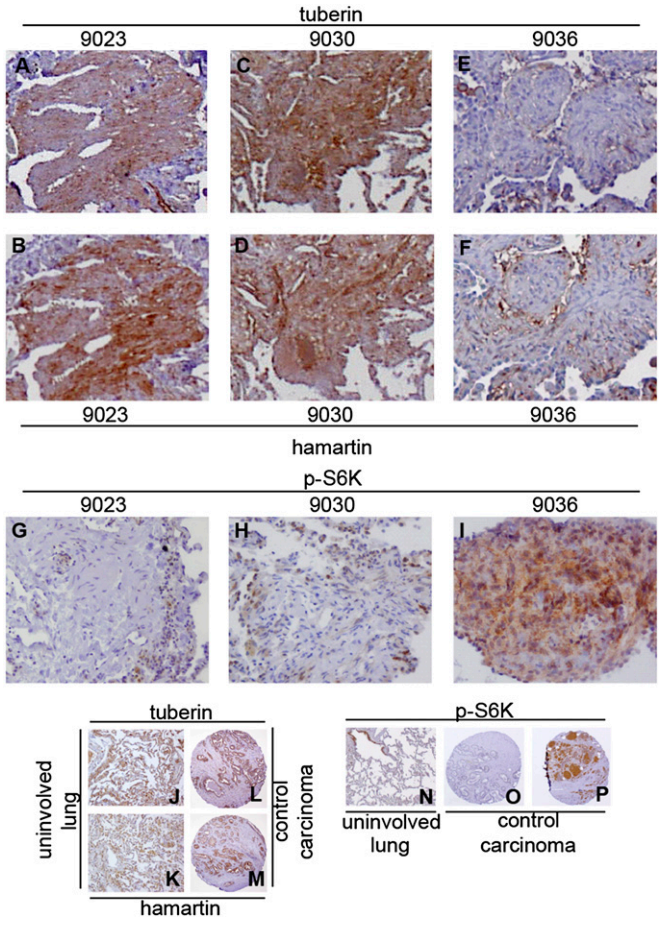

Figure 1. Hamartin and tuberin expression and lack of phosphorylated S6K (p-S6K) expression in lymphangioleiomyomatosis (LAM) nodules from two LAM cases with no mutation identified. Three LAM lesions are shown. (*A–D*) Two cases, 9023 and 9030, had no mutations found in either *TSC1* or *TSC2*, and expressed hamartin and tuberin. (*E* and *F*) In contrast, case 9036 had no expression of those proteins, and had a high level of *TSC2* mutation with LOH. (*G–I*) Cases 9023 (*G*) and 9030 (*H*) do not express p-S6K, whereas case 9036 (*I*) shows strong p-S6K immunopositivity. (*J* and *K*) Hamartin and tuberin expression in uninvolved lung parenchyma and (*L* and *M*) in prostate carcinoma (from tissue array control included in every slide). (*N–P*) p-S6K expression in uninvolved lung parenchyma (note + reactive alveolar epithelium in *upper left corner*), prostate carcinoma (negative), and breast carcinoma (positive), respectively. Original magnifications, ×100.

Author Contributions: K.R.B., X.Z., D.J.K, and L.S. contributed to study conception and design; K.R.B., W.Q., L.G., X.Z., N.S., E.H., D.J.K., and L.S. contributed to conduct research; K.R.B., W.Q., L.G., Y.C., E.H., D.J.K., and L.S. contributed to analyze and interpret data; K.R.B., D.J.K, and L.S. drafted the manuscript and all authors contributed to the report and approved the version submitted.

Supported by NHLBI/NIH grants HL077514 (to L.S.), HL048730 (to L.S.), and RC1 HL100655-01 (to D.J.K.), NINDS/NIH grant 2R37NS031535-14 (to D.J.K.), and the LAM Treatment Alliance (to D.J.K.). K.R.B. is an American Lung Association Interstitial Lung Disease Scholar (Dalsemer Research Grant, DA-196629-N).

This article has an online supplement, which is accessible from this issue's table of contents at www.atsjournals.org

TABLE 1. MUTATIONS AND SINGLE-NUCLEOTIDE POLYMORPHISMS DETECTED IN *TSC1* AND *TSC2* IN 10 SPORADIC LAM SAMPLES

Sample	Method	TSC2 Mutation	Allelic Frequency	Mutation Effect	TSC2 SNPs	LOH	MLPA Copy #	TSC1	HMB45 Expression*
9016	Illumina	c.5024C > T	16%	p.1675P > L missense	2	No	ND	ND	5+
9020	454	c.781C > T	50%	p.261R > W missense	1	No	NL	ND	1+
	454	c.3610+1G > A	15%	Splice					
9022	454	c.789_806del18	8%	In-frame deletion	0	No	NL	ND	3+
9023	454	None			3	No	NL	None†	5+
9030	454	None			1	No	NL	None	1+
9034	454	c.5127delC	39%	Truncation	4	No	NL	ND	1+
					2580T>C	Yes‡			
9036	454	c.1947-4_2030del88	60%	Truncation	1	Yes§	NL	ND	1+
9038	454	c.1837C>T	4%	p.Q613X	1	No	NL	ND	2+
9043	Illumina	c.3167delG	18%	Truncation	14	Yes¶	NL	ND	1+
9059	Illumina	c.1513C>T	16%	p.R505X	5	No	NL	ND	1+

Definition of abbreviations: LAM = lymphangioleiomyomatosis; LOH = loss of heterozygosity; MLPA = multiplex ligation-dependent probe assay; ND = not done; NL = normal; SNPs = single-nucleotide polymorphisms.

*HMB45 expression is scored on a qualitative scale from 1+ (weak) to 5+ (strong).

†This sample had one TSC1 SNP.

‡This sample showed a 2:1 allelic ratio in sequencing reactions, consistent with LOH, but only for one of five heterozygous SNPs found in this sample.

§This sample showed evidence for LOH by Sanger sequencing of the deletion mutation, in that there was increased frequency of the deletion allele in comparison to the wild-type allele.

¶LOH was seen in this sample, with a skewed allele ratio for 14 TSC2 intragenic SNPs, for which the average minor allele frequency was 0.42 in comparison to an average minor allele frequency of 0.47 for control sample SNPs ($P < 0.001$).

a frequency less than 20%. All were verified by Sanger or SNaPshot analysis on unamplified DNA (Figures E6 and E7). Four samples showed evidence of two-hit inactivation in *TSC2*, three of them with a mutation and LOH, and one with two point mutations. The four cases without LOH all had low allele fractions for mutation in TSC2 (≤16%), making detection of LOH difficult. The two LAM samples in which no *TSC2* mutation was identified also showed no mutation in *TSC1* by NGS sequencing. Significantly, in one of these cases, over 90% of LAM cells were positive for HMB45 (case 9023) (Figure E8B), and in the other, the patient had a concomitant renal angiomyolipoma, providing additional evidence of S-LAM (1, 2). $HMB45^+$ cells in LAM sections have relatively low PCNA expression, suggesting that they are less proliferative than $HMB45^-$ cells (14). Although some types of inactivating mutations are missed by exonic sequencing, immunohistochemistry for TSC2 (tuberin) and TSC1 (hamartin) on the two cases without defined mutations showed strong expression of each protein, whereas little or no expression of either was seen in a control case with two mutations in *TSC2* (Figure 1 and Figure E10). Furthermore, the two cases without TSC1/TSC2 mutation showed no expression of phospho-S6 kinase by immunohistochemistry, in contrast to cases in which biallelic TSC2 mutations were identified (Figures 1G–1I). This suggests that mechanistic target of rapamycin complex 1 (mTORC1) was not activated in the LAM nodules of these two patients, consistent with normal TSC1/TSC2 function and mTOR regulation.

The occurrence of *TSC2* mutations at relatively low frequency, or not at all, in these LAM samples is surprising. As shown here and elsewhere (13), NGS has the capability to detect mutations that are present at a very low allelic fraction, 1% or lower, enabling high sensitivity analyses as performed here. High sample contamination with non-LAM cells seems unlikely given our efforts at histological purification of the cells collected by LCM, the identification of mutations at high frequency in some cases, and the detection of a low- and a high-frequency mutation in one case. It is possible that *TSC2* mutations occur in a subset of LAM cells, after other unknown initiating events, and are not the primary driver of LAM development, or TSC2-mutant cells recruit stromal cells to adopt an SMA-positive phenotype. In addition, the two cases without *TSC1* or *TSC2* mutations identified also suggest that alternative genetic mechanisms may be operative in some cases of LAM.

Recently the Multicenter International LAM Efficacy of Sirolimus (MILES) trial demonstrated that rapamycin (sirolimus), an mTORC1 inhibitor that blocks the pathway activated by loss of tuberin (15), was an effective therapy for treatment of LAM (16). However, it is notable that continuing FEV_1 decline was seen in 50% of patients on rapamycin therapy. It is possible that some of these nonresponders do not have loss of TSC2 with activation of mTORC1 as a fundamental pathogenic mechanism for LAM development, consistent with our data.

Author disclosures are available with the text of this letter at www.atsjournals.org.

Kameswara Rao Badri, Ph.D.*†
Ling Gao, M.D.
Elizabeth Hyjek, M.D.
Noa Schuger, B.A.
Lucia Schuger, M.D.‡
University of Chicago
Chicago, Illinois

Wei Qin, Ph.D.*
Yvonne Chekaluk, M.S.
David J. Kwiatkowski, M.D., Ph.D.‡
Brigham and Women's Hospital
Boston, Massachusetts
and
Harvard Medical School
Boston, Massachusetts

Xiaoning Zhe, M.D., Ph.D.
Wayne State University
Detroit, Michigan

References

1. Cohen MM, Pollock-BarZiv S, Johnson SR. Emerging clinical picture of lymphangioleiomyomatosis. *Thorax* 2005;60:875–879.

*These authors contributed equally to this work.

† Present address: OSRA, Savannah State University, 3219 College Street, Savannah, GA 31404.

‡ These authors contributed equally to this work.

2. Taveira-DaSilva AM, Pacheco-Rodriguez G, Moss J. The natural history of lymphangioleiomyomatosis: markers of severity, rate of progression and prognosis. *Lymphat Res Biol* 2010;8:9–19.
3. McCormack FX. Lymphangioleiomyomatosis: a clinical update. *Chest* 2008;133:507–516.
4. Hohman DW, Noghrehkar D, Ratnayake S. Lymphangioleiomyomatosis: a review. *Eur J Intern Med* 2008;19:319–324.
5. Seyama K, Kumasaka T, Kurihara M, Mitani K, Sato T. Lymphangioleiomyomatosis: a disease involving the lymphatic system. *Lymphat Res Biol* 2010;8:21–31.
6. Carsillo T, Astrinidis A, Henske EP. Mutations in the tuberous sclerosis complex gene TSC2 are a cause of sporadic pulmonary lymphangioleiomyomatosis. *Proc Natl Acad Sci USA* 2000;97:6085–6090.
7. Sato T, Seyama K, Fujii H, Maruyama H, Setoguchi Y, Iwakami S, Fukuchi Y, Hino O. Mutation analysis of the TSC1 and TSC2 genes in Japanese patients with pulmonary lymphangioleiomyomatosis. *J Hum Genet* 2002;47:20–28.
8. Goncharova EA, Goncharov DA, Eszterhas A, Hunter DS, Glassberg MK, Yeung RS, Walker CL, Noonan D, Kwiatkowski DJ, Chou MM, *et al*. Tuberin regulates p70 S6 kinase activation and ribosomal protein S6 phosphorylation: a role for the TSC2 tumor suppressor gene in pulmonary lymphangioleiomyomatosis (LAM). *J Biol Chem* 2002;277:30958–30967.
9. Crooks DM, Pacheco-Rodriguez G, DeCastro RM, McCoy JP Jr, Wang JA, Kumaki F, Darling T, Moss J. Molecular and genetic analysis of disseminated neoplastic cells in lymphangioleiomyomatosis. *Proc Natl Acad Sci USA* 2004;101:17462–17467.
10. Cai X, Pacheco-Rodriguez G, Fan QY, Haughey M, Samsel L, El-Chemaly S, Wu HP, McCoy JP, Steagall WK, Lin JP, *et al*. Phenotypic characterization of disseminated cells with TSC2 loss of heterozygosity in patients with lymphangioleiomyomatosis. *Am J Respir Crit Care Med* 2010;182:1410–1418.
11. Badri KR, Qin W, Gao L, Zhe X, Gong C, Schuger N, Hyjek E, Kwiatkowski DJ, Schuger L. A subgroup of lymphangioleiomyomatosis with no TSC mutations identified [abstract]. *FASEB J* 2012;26:Ib498.
12. Badri KR, Gao L, Gong C, Qin W, Kwiatkowski DJ, Schuger N, Schuger L. Lack of exonic mutations TSC1/TSC2 mutations is not uncommon in sporadic LAM [abstract]. Presented at the First European LAM Conference. October 1–3, 2010, Udine, Italy.
13. Qin W, Kozlowski P, Taillon BE, Bouffard P, Holmes AJ, Janne P, Camposano S, Thiele E, Franz D, Kwiatkowski DJ. Ultra deep sequencing detects a low rate of mosaic mutations in tuberous sclerosis complex. *Hum Genet* 2010;127:573–582.
14. Matsumoto Y, Horiba K, Usuki J, Chu SC, Ferrans VJ, Moss J. Markers of cell proliferation and expression of melanosomal antigen in lymphangioleiomyomatosis. *Am J Respir Cell Mol Biol* 1999;21:327–336.
15. Kwiatkowski DJ, Manning BD. Tuberous sclerosis: a GAP at the crossroads of multiple signaling pathways. *Hum Mol Genet* 2005;14 (Spec 2):R251–R258.
16. McCormack FX, Inoue Y, Moss J, Singer LG, Strange C, Nakata K, Barker AF, Chapman JT, Brantly ML, Stocks JM, *et al*. Efficacy and safety of sirolimus in lymphangioleiomyomatosis. *N Engl J Med* 2011;364:1595–1606.

ONLINE DATA SUPPLEMENT

Methods

Histological analysis of formalin-fixed samples

Three or more paraffin blocks from at least 2 different lung lobes were analyzed per case. Serial 4 μm sections were stained with Hematoxylin and Eosin (H&E), cut for immunohistochemistry studies, and stained with Masson-trichrome stain from each block following protocols in routine use in our diagnostic pathology lab. Collagen was identified by Masson trichrome staining using the Trichrome II Blue Staining Kit (Ventana Medical Systems, Tucson, AZ), in accordance with the manufacturer's instructions. Monoclonal mouse antibodies against human: smooth muscle actin (SMA) (clone 1A4; cat. no. M0851), lymphocytes (CD45, clones 2B11+ PD7/26; cat. no. M0701), lymphatic endothelium (clone D2-40; cat. no. M361959), gp100 (clone HMB45, cat. no. M0634) and vascular endothelium (CD31, clone JC70A, cat. no. M0823) were purchased from DAKO North America (Carpinteria, CA). Immunohistochemistry was performed on the automated Bond ^{TM} system (Leica-Microsystems, Buffalo Grove, IL) according to the modified manufacturer protocol, including 25 min incubation with primary antibodies, 15 min post-primary step and 25 min incubation with HRP- polymer using Bond ^{TM} Polymer Refine Detection system (Leica Biosystems Newcastle Ltd), following heat antigen retrieval. The peroxidase reaction was developed using 3,3 diaminobenzidine (DAB) provided in the kit. Polyclonal rabbit antibodies against tuberin (Santa Cruz, CA, cat. no. SC-893), hamartin (Abcam, cat. no. AB25882) and p-S6K (Abcam, cat. no. ab59208) were used at 1:100 dilution according to standard protocols used in diagnostic pathology

lab. The slides were examined and interpreted by 2 independent pathologists (E. H. and L.S.).

Next generation sequencing (NGS)

454 NGS

Whole genome amplified DNA (WGA-DNA) from LAM lesions was analyzed for mutations in *TSC1* and *TSC2* using deep sequencing by the 454 technique (Roche Applied Sciences, Indianapolis, IN), as described in detail elsewhere (1). In brief, exons were amplified using specially designed oligonucleotide primers, consisting of a 15-28 bp target-specific sequence at their 3′ end, and a common 19 bp region that was used in subsequent clonal amplification and sequencing reactions at their 5′ end. Amplicons ranged in size from 135 to 393 bp. PCR was performed on 10-25 ng of WGA-DNA using the FastStart High Fidelity PCR System (Roche Applied Sciences) and standard thermocycling conditions. Amplicon products were purified, quantified, and pooled at an equimolar ratio for sequencing. Single molecules were clonally amplified on beads in an oil emulsion; beads were then isolated and loaded into picotiter plates for pyrosequencing (2, 3). Individual patient samples were multiplexed in sets of 8, and sequencing was performed on the Genome Sequencer FLX system (Roche Applied Sciences). The median and mean number of reads was 486 and 506, respectively, at the coding and splice site nucleotides of *TSC2.* 95.5% of amplicons had a read depth >200, and 98.6% had a read depth >100.

454 sequence data was analyzed using Amplicon Variant Analysis (AVA; Roche Applied Sciences) software to identify sequence variants in *TSC1* and *TSC2*. As described

previously (1), many low-frequency sequence variants are detected in 454 analyses, and we eliminated from further consideration those variants that were: (1) detected in >1 sample at low frequency; (2) detected in <5 sequencing reads; and (3) detected only in poor quality reads by manual review.

Illumina NGS

Next generation sequencing of most of the genomic extent of *TSC2* was performed on the Illumina GAIIx or HiSeq2000 (Illumina, San Diego, CA). Long-range PCR was performed on LAM WGA-DNA using 4 primer sets that cover all of the coding exons and most of the intronic sequence of *TSC2,* a total of 34,770 nt. Amplicons were then purified using AMPure beads and used to prepare a small fragment library for Illumina sequencing. Amplicons were concatenated by ligation with T4 DNA Ligase, purified, and sheared in a Covaris E210 instrument at settings of 10% duty cycle, intensity of 5, and 150 cycles per burst to a size of 200-400 bp (Covaris, Woburn, MA). Sheared DNA was then end-repaired with the End-It kit (Epicenter, Madison, WI), A-tailed with Klenow, and purified using AMPure beads. Illumina adaptors were annealed and ligated. Fragments were minimally amplified, purified using AMPure beads, minimally reamplified with primers encoding an index sequence (Illumina), and purified using AMPure beads. Libraries from different samples with different indices were then mixed at an equimolar ratio and sequenced on an Illumina GAIIx or HiSeq2000 sequencer for 50-75 nt reads.

Sequencing data output was analyzed using a combination of standard tools and custom software to enable detection of sequence variants at >1% frequency. The primary data were deconvoluted using the index sequences to individual sample files and converted to FASTQ format, aligned to the human genome using bwa-0.5.8c (Burrows-Wheeler

Alignment) (2), filtered to eliminate reads of low quality and to reduce redundancy to a uniform 50 reads starting at each nucleotide position of interest in each direction (C. Pedamallu, Broad Institute), sorted and converted to bam and bai files using Picard tools. The data were then analyzed for sequence variants using tools from the Genome Analysis Toolkit (GATK) (3), including IndelGenotyperV2 and Unified Genotyper, to identify both indels and single nucleotide variants. A second approach was used in parallel to analyze the sequence data, with capture of read calls at all positions using Pileup (SAMtools) and GetCalls (M. Lawrence, Broad Institute); those data were then analyzed in Matlab. The output from these analyses was reviewed in comparison with those from other samples, including controls, to exclude artifacts derived from the sequencing process. All variants seen at a frequency of $\geq$1% more than that seen in other samples were directly reviewed using the Integrative Genomics Viewer (4) (IGV; www.broadinstitute.org/software/igv/) to help confirm bona fide variant calls and to exclude sequencing artifacts. A median read depth for all nucleotides of the *TSC2* coding exons and nearby introns of >2,000 was achieved by Illumina NGS, and >94% of these nucleotides were covered at a read depth of >1,000.

Validation of NGS findings

Single-nucleotide variants and indels that were identified as novel and/or of possible significance by either 454 or Illumina NGS were confirmed by secondary analysis of the initial non-WGA DNA sample, using Sanger bidirectional sequencing in the case of variants seen at > 20% allele ratio and SNaPshot analysis for those seen at <20% allele ratio. SNaPshot analysis was performed as described elsewhere (1). Primer extension products were analyzed on an ABI 3100 sequencer (Applied Biosystems, Carlsbad, CA), and the proportion of alleles was quantified using GeneMapper version 3.0 (Applied

Biosystems). In this analysis, small peaks were seen for variant nucleotides in some cases because of spontaneous base misincorporation. However, comparison with control samples permitted discrimination of bona fide variants at allele frequencies as low as 5% or less. The allele frequency of mutant alleles was determined as M/(M + W), where M and W are the peak areas of the mutant and wild-type allele products, respectively, after subtraction of the signal seen in control samples. All SNaPshot experiments were replicated at least once.

Supplemental Figure Legends

Supplemental Figure E1. Laser capture microdissection (LCM) of nodular lymphangioleiomyomatosis (LAM) lesions. A, Reference slide of a LAM lesion immunostained for smooth muscle α-actin (SMA); narrow strips (arrows) were avoided. B, Slide of a representative LAM lesion with hematoxylin and eosin (H&E) stain used for LCM. C, Slide shown in panel B after LCM was performed. D, Slide of a representative LAM lesion with H&E stain showing the laser (pink line). E, Inset shown in panel D. F, Slide shown in panel D after LCM was performed. Magnifications: A-C: X 100, D: X 200, E, F: X 400.

Supplemental Figure E2. Differences in the expression of melanocytic protein gp100 (HMB-45) in representative lymphangioleiomyomatosis (LAM) lesions. The highest proportion of HMB45–positive cells (>90% of all LAM cells) was seen in case 9023 (C), whereas the lowest proportion of HMB-45-positive cells (<5% of all LAM cells) was seen in case 9030 (F). A, D, LAM lesions stained with hematoxylin and eosin (H&E). B, E, LAM lesions stained for smooth muscle α-actin (SMA), showing that the lesions are largely composed of SMA-positive cells (brown). C, F, LAM lesions stained for HMB-45.

Cells positive for HMB-45 (brown) were identified in all lesions, varying in number both between cases and between lesions within the same case. Magnifications: X 100.

Supplemental Figure E3. Lymphatic channels and lymphatic endothelial differentiation in lymphangioleiomyomatosis (LAM) lesions. H&E examination and IHC with antibody D2-40 against podoplanin (a marker for lymphatic endothelium) demonstrated that LAM lesions contained few to multiple lymphatic channels of various diameters (brown), some of them with slit-like lumens (D, arrows). Nevertheless, the overall lymphatic channel density was similar among the 10 cases. A-C are H&E, SMA, and HMB-45 immunostaining of corresponding serial sections from case 9016. Surprisingly, in all cases numerous LAM cells showed staining for D2-40, albeit weaker than lymphatic endothelial cells (D). Magnifications: X 100.

Supplemental Figure E4. Variable presence of lymphocytes in lymphangioleiomyomatosis (LAM) lesions. LAM lesions contained lymphocytes in all 10 cases, ranging from few (A-D) to multiple (E and inset with arrows pointing at lymphocytes) to numerous (F). A, C, E, F, Hematoxylin and eosin stain (H&E); B, D, Anti-CD45 stain for lymphocytes (brown). Lymphocytes are found either diffuse (E) or in clusters (F). When the lymphocytes were numerous the portions of LAM lesions or entire LAM lesion were not collected. Magnifications: X 100**.**

Supplemental Figure E5. Collagen deposition in LAM. Two lesions are shown, case #9036 (left, non-collagenized) and 9038 (right, high collagenization). A, E, Hematoxylin and eosin (H&E) stain; B,F, anti-smooth muscle α-actin (SMA) stain; C, G, anti-melanocytic protein gp100 (HMB45) stain; D, H, Masson-Trichrome stain for collagen (blue). Most of the collagenized areas are acellular or contain a small number of spindle-

shaped cells, which are generally positive for SMA and HMB45 (brown) and therefore consistent with LAM cells. Magnifications: X 100.

Supplemental Figure E6. Sequencing confirmation of a large deletion in TSC2 and an LOH event. A, Sequencing analysis shows that a large deletion in TSC2 (del1947-4-2030) was more common thant the wild type allele in sample 9036. B, Sequencing analysis shows unbalanced allelic representation in the SNP 2580T>C of TSC2 in sample 9034.

Supplemental Figure E7. Confirmation of mosaic mutations in TSC2 by SNaPshot single base extension sequencing. LAM (top) and control (bottom) samples are shown for 4 different mutations in TSC2 detected by deep sequencing. The mutant allele frequency is shown as percent for each sample.

Supplemental Figure E8. Lymphangioleiomyomatosis (LAM) histology and immunohistochemistry analyses. A-D, F. Representative LAM lesions from all 10 LAM cases, shown in pairs. Top panel, Hematoxylin and eosin (H&E) stain; Middle panel, anti–smooth muscle α-actin (SMA) stain; Lower panel, anti–melanocytic protein gp100 (HMB45) stain. E: high magnification of inset from figure 1D showing HMB-45 positive cells (*brown*, arrows). G: high magnifications of insets 1-3 from figure 1F. Upper left inset shows HMB-45 positive cells (arrows) in case 9043. Upper right inset shows a LAM lesion in case 9059 demarcated in green. LAM lesions in this case are not clearly distinguished at the low magnification shown in previous figure. Lower right inset shows HMB-45 positive cells (*brown*) in same lesion. Magnifications: X100, insets: X 400.

Supplemental Figure E9. Location of most lymphocytes in aggregates outside LAM lesions. Lymphocyte aggregates were common in all LAM lung specimens, either in clusters (A–D), near blood vessels (C), and bronchi (D) or diffusely thickening (E, F) the alveolar wall. A–E, Representative LAM lesions stained with hematoxylin and eosin (H&E) and F, with anti-CD45 for lymphocytes (*brown*). Magnifications: X100.

Supplemental Figure E10. LAM lesions from case 9036 (highest mutation frequency rate and LOH) are either negative for tuberin (A) or show sparsely distributed tuberin-positive cells (B). Control case 9023 (NMI) shows presence of tuberin in all LAM cells (C).

References

1. Qin W, Kozlowski P, Taillon BE, Bouffard P, Holmes AJ, Janne P, Camposano S, Thiele E, Franz D, Kwiatkowski DJ. Ultra deep sequencing detects a low rate of mosaic mutations in tuberous sclerosis complex. *Hum Genet* 2010;127:573-582.

2. Li H, Durbin R. Fast and accurate long-read alignment with burrows-wheeler transform. *Bioinformatics* 2010;26:589-595.

3. McKenna A, Hanna M, Banks E, Sivachenko A, Cibulskis K, Kernytsky A, Garimella K, Altshuler D, Gabriel S, Daly M, DePristo MA. The genome analysis toolkit: A mapreduce framework for analyzing next-generation DNA sequencing data. *Genome Res* 2010;20:1297-1303.

4. Robinson JT, Thorvaldsdottir H, Winckler W, Guttman M, Lander ES, Getz G, Mesirov JP. Integrative genomics viewer. *Nat Biotechnol* 2011;29:24-26.

Supplemental Figure E1

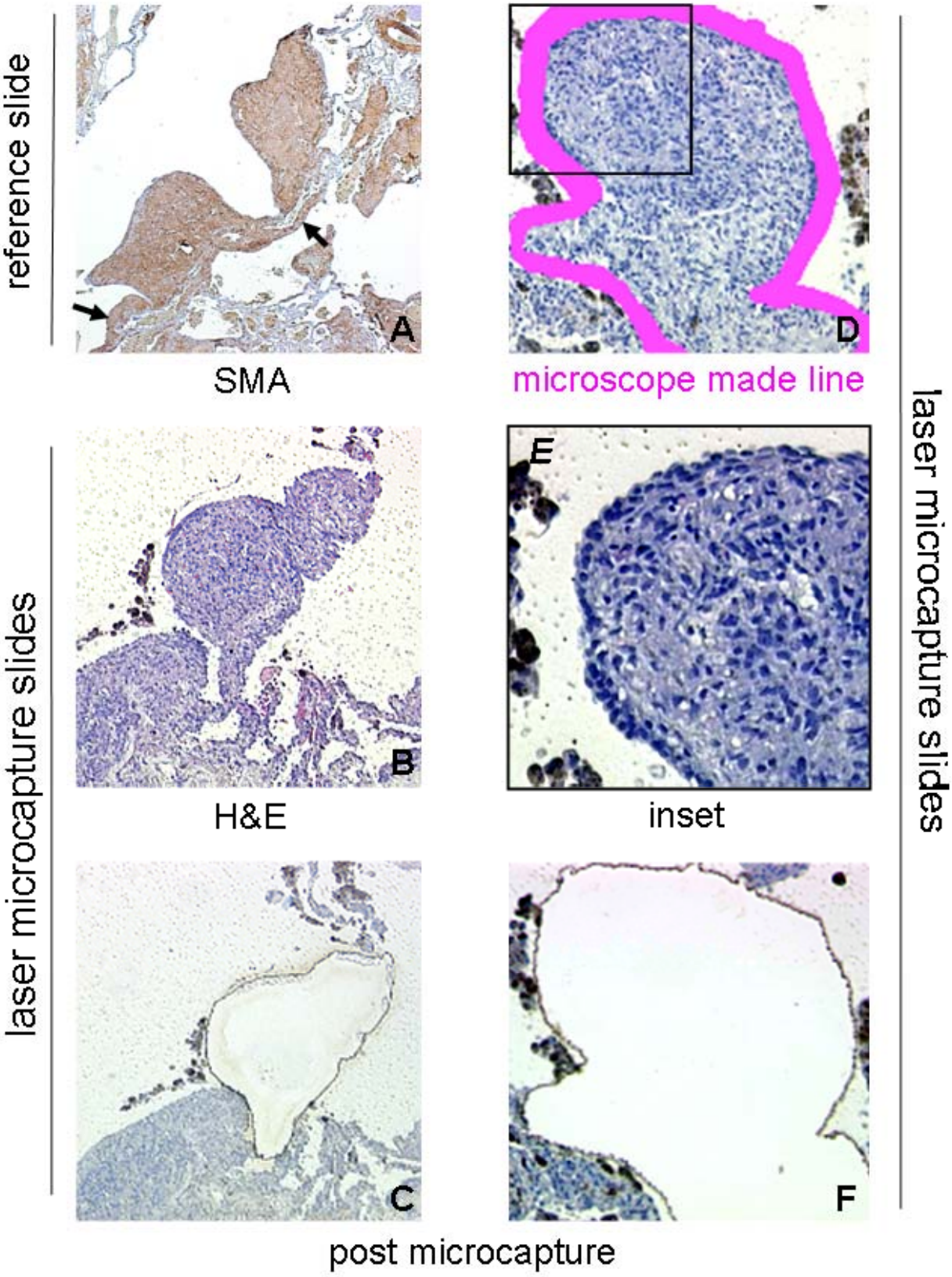

Supplemental Figure E2

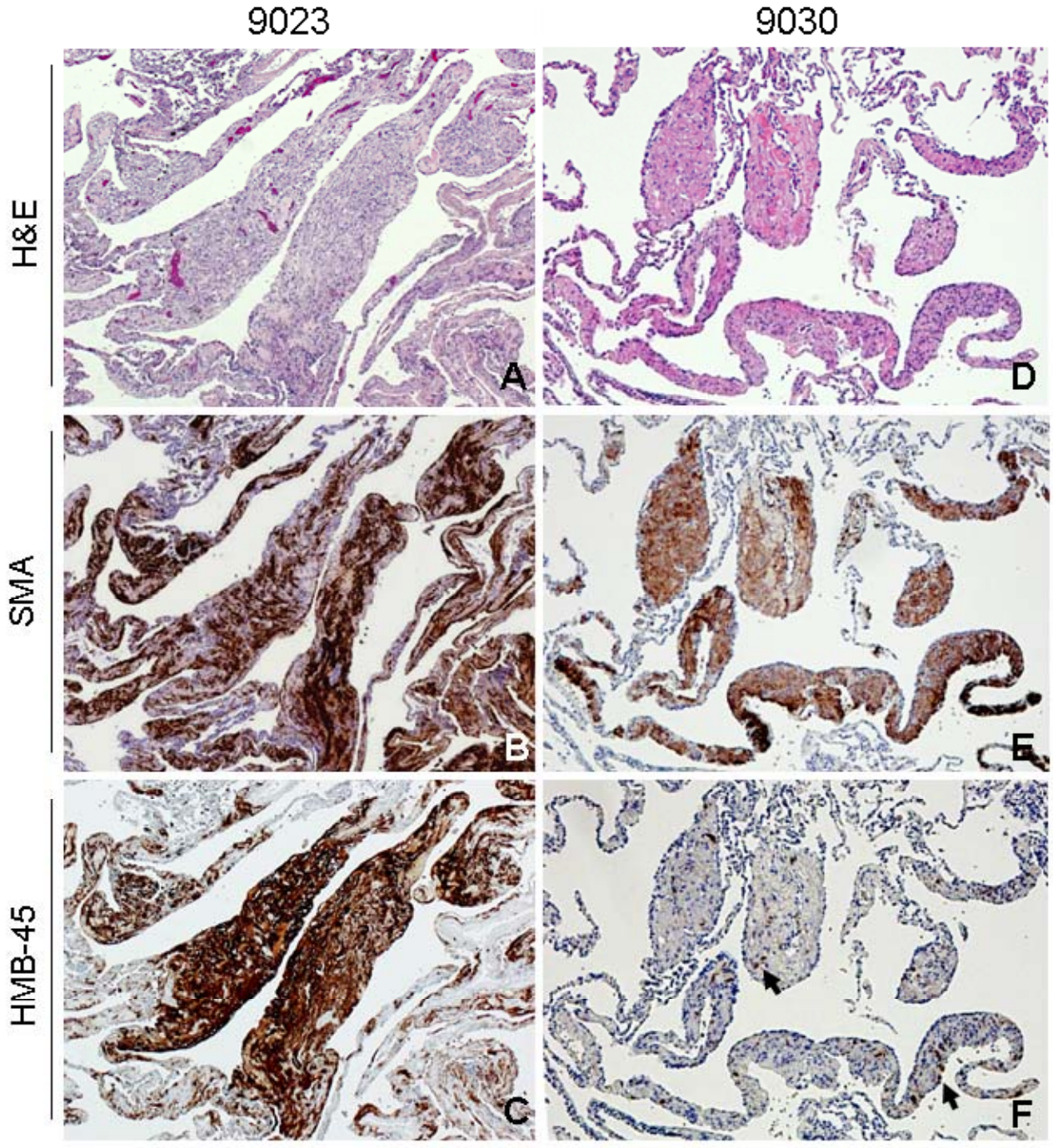

Supplemental Figure E3

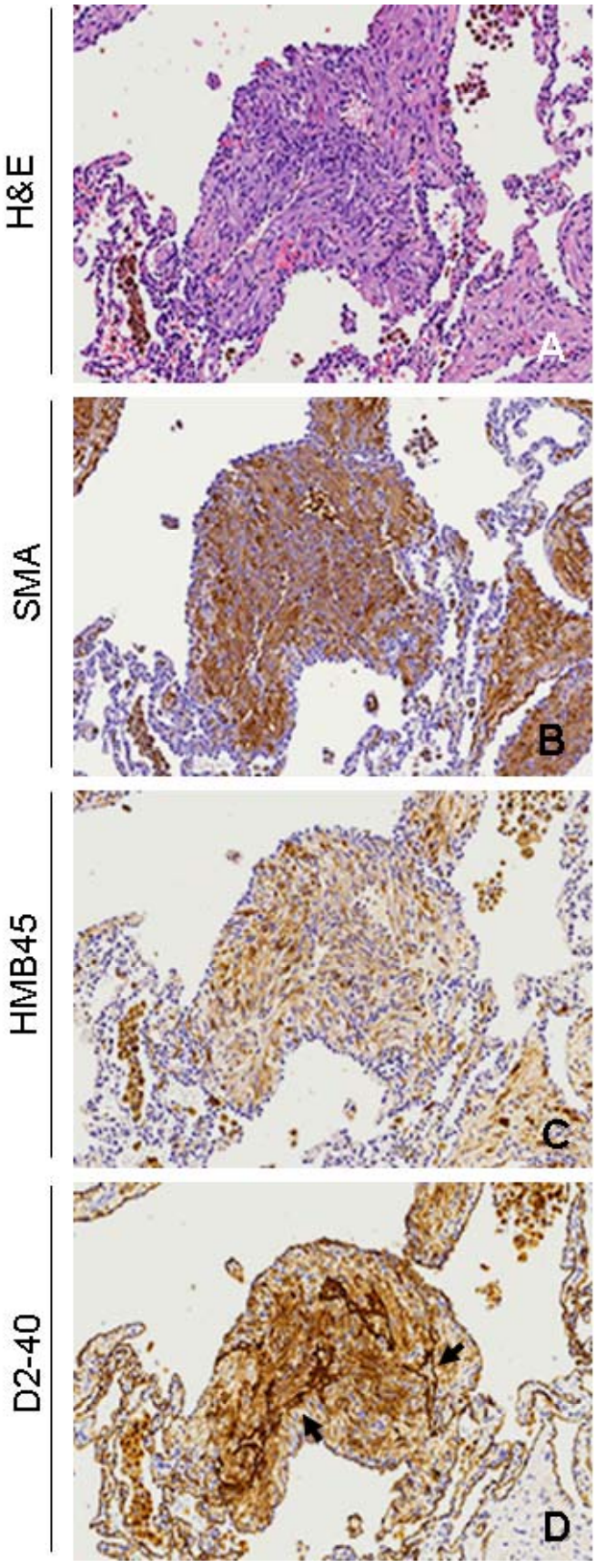

Supplemental Figure E4

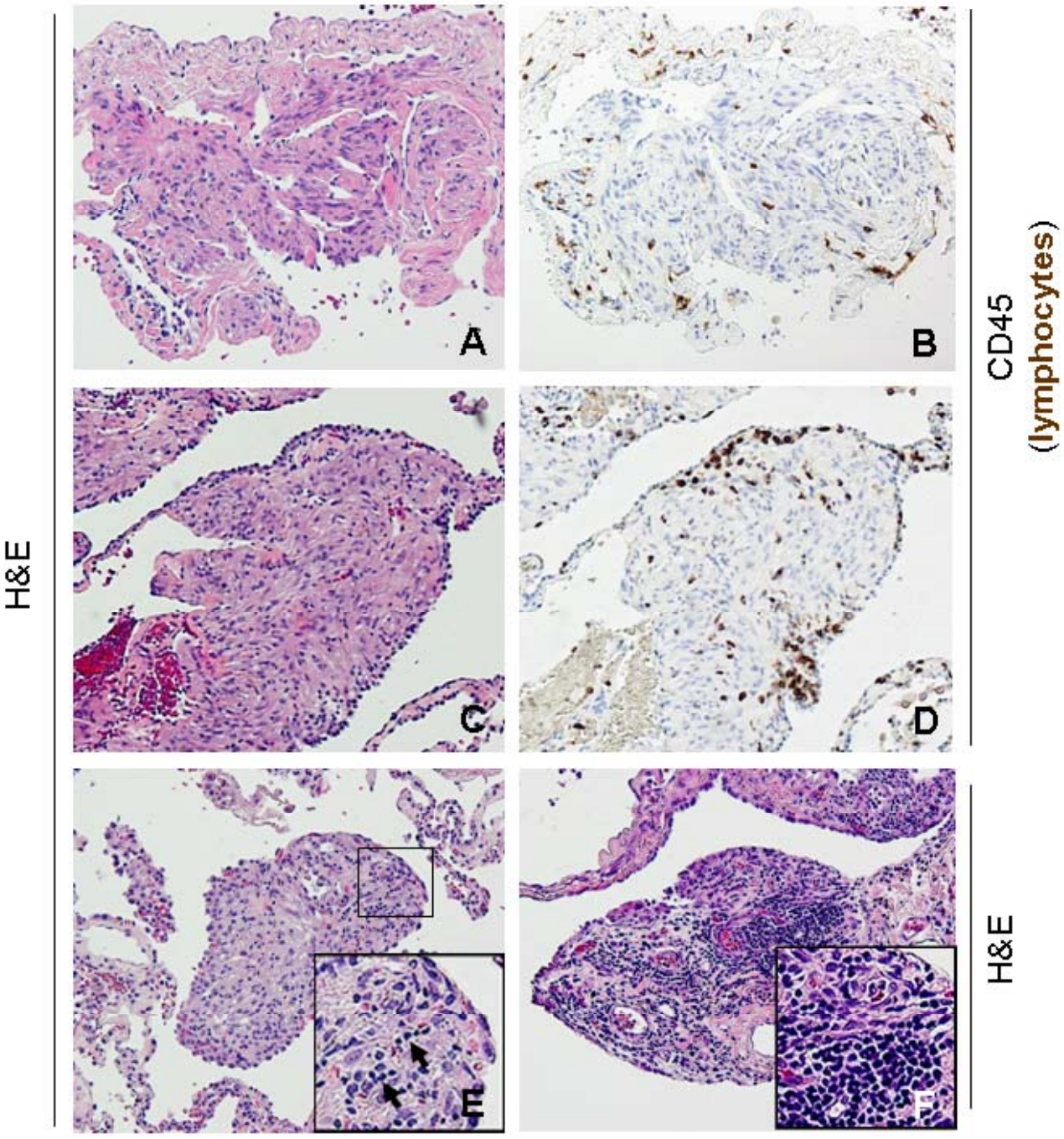

Supplemental Figure E5

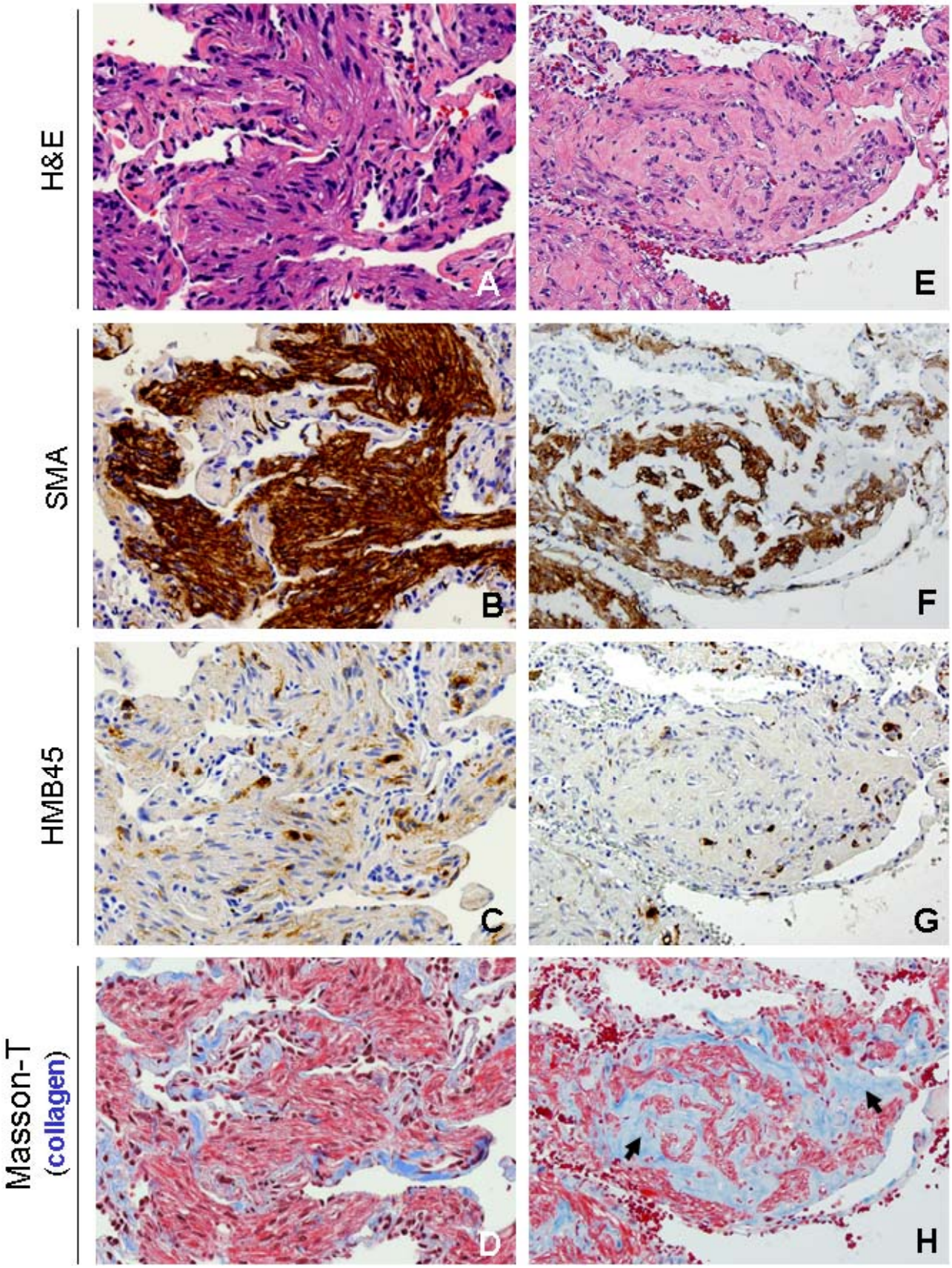

Supplemental Figure E6

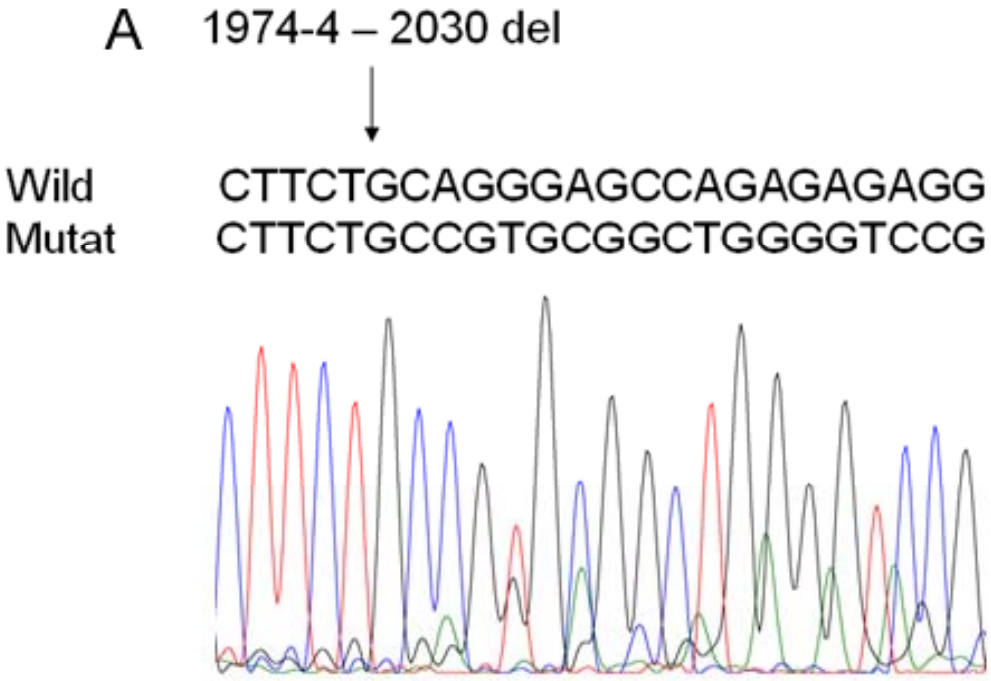

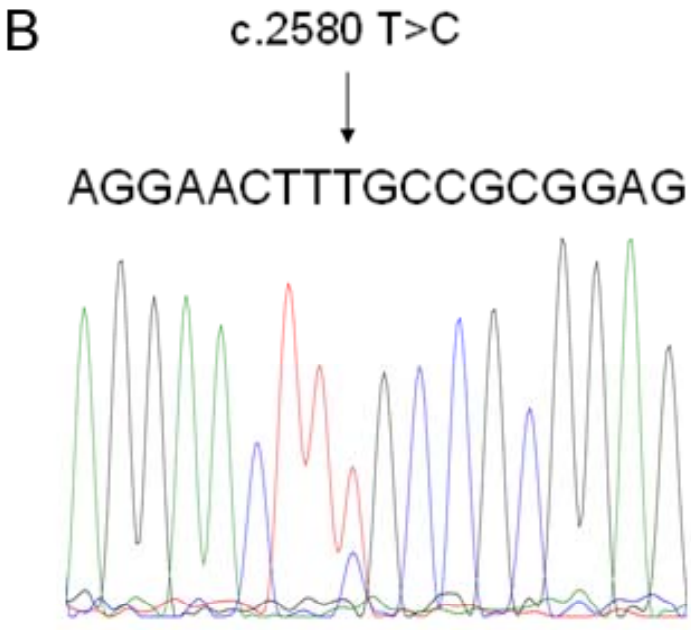

Supplemental Figure E7

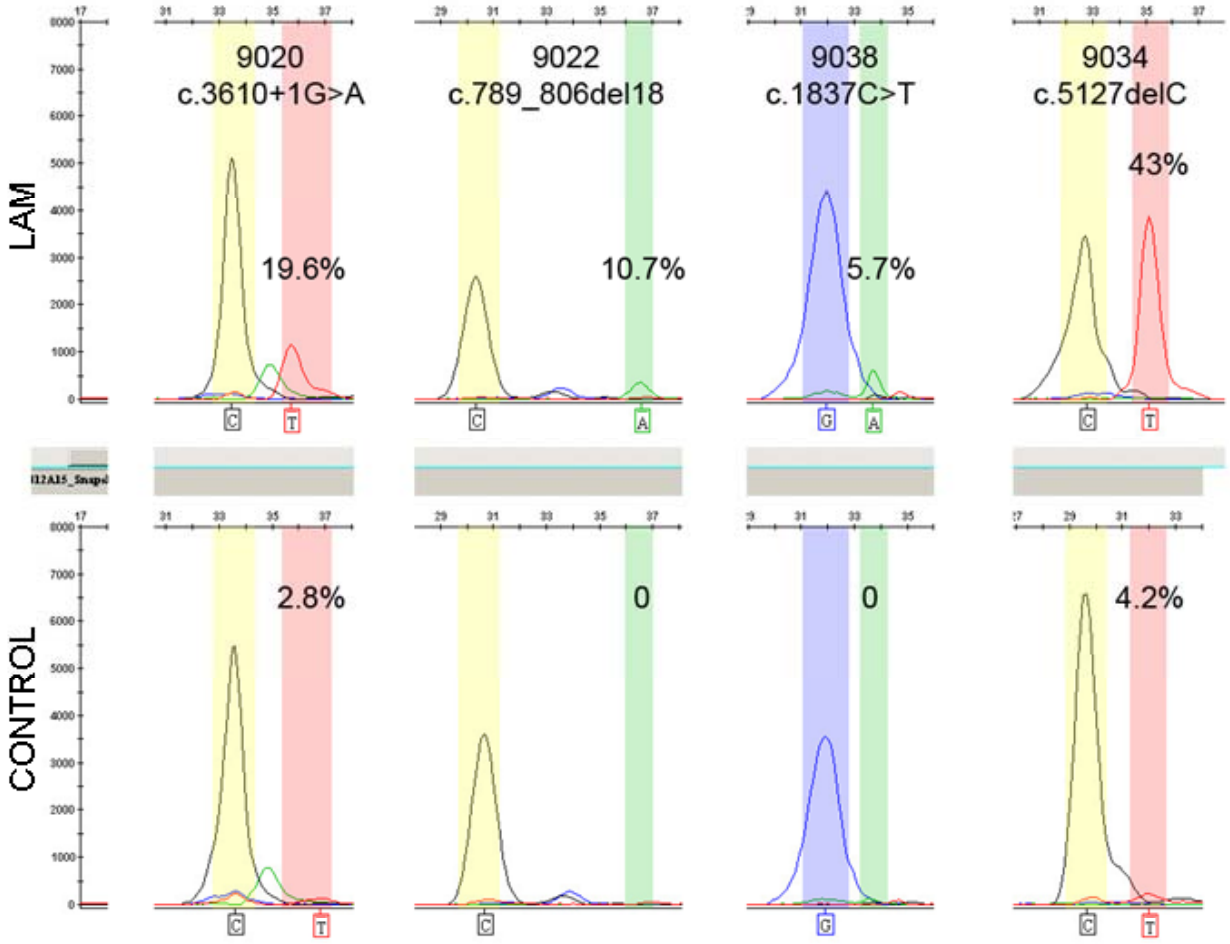

Supplemental Figure E8A

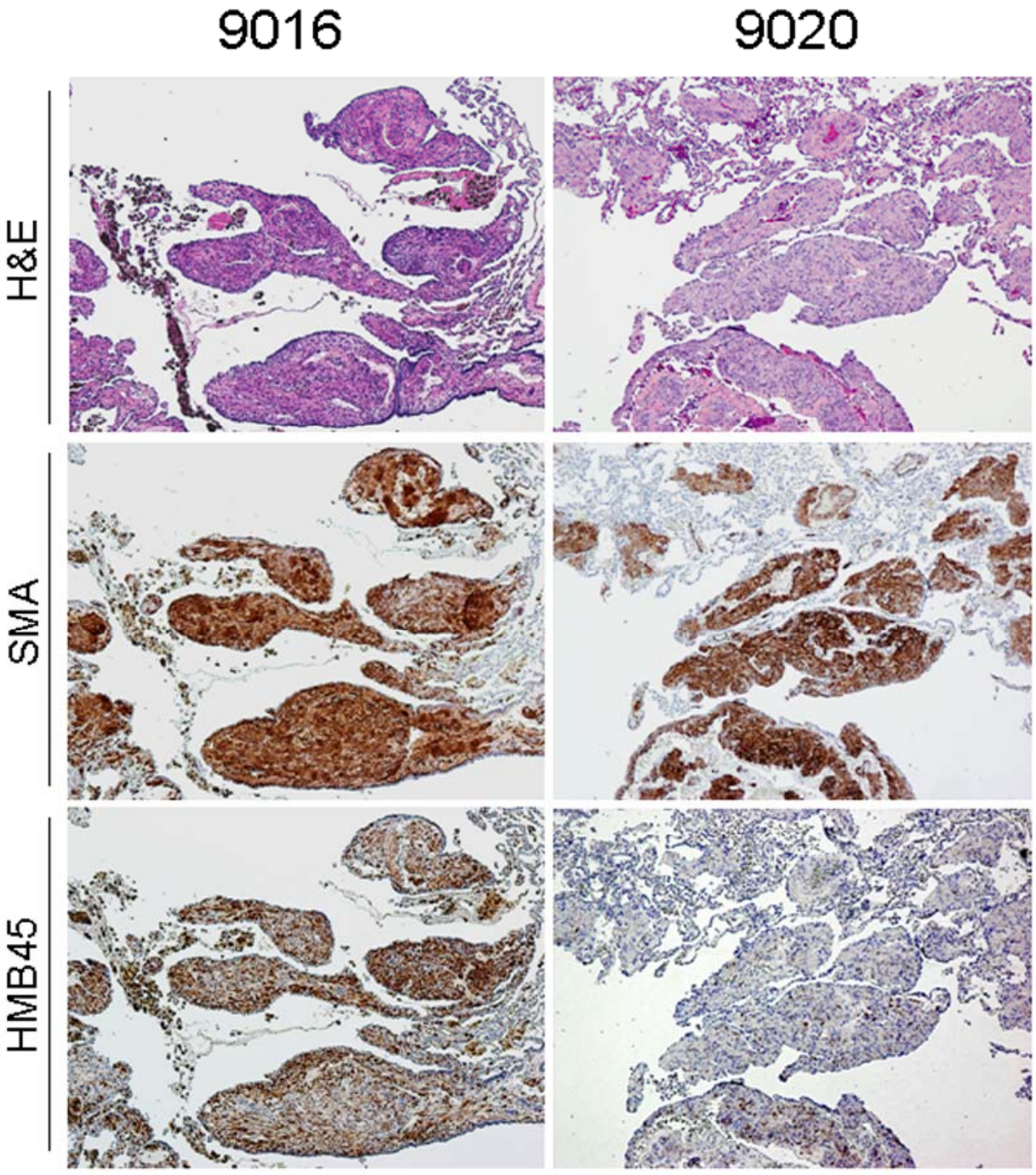

Supplemental Figure E8B

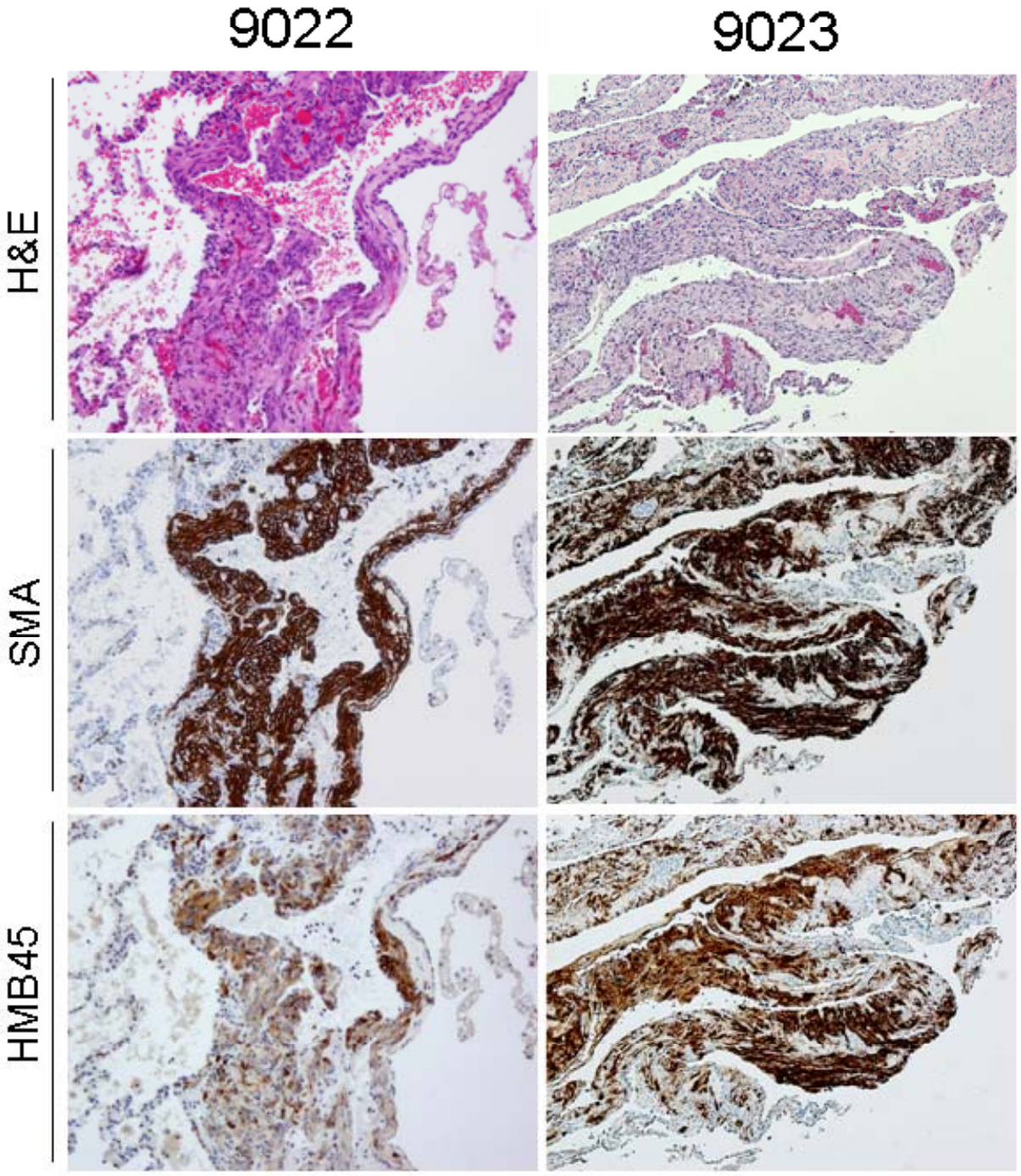

Supplemental Figure E8C

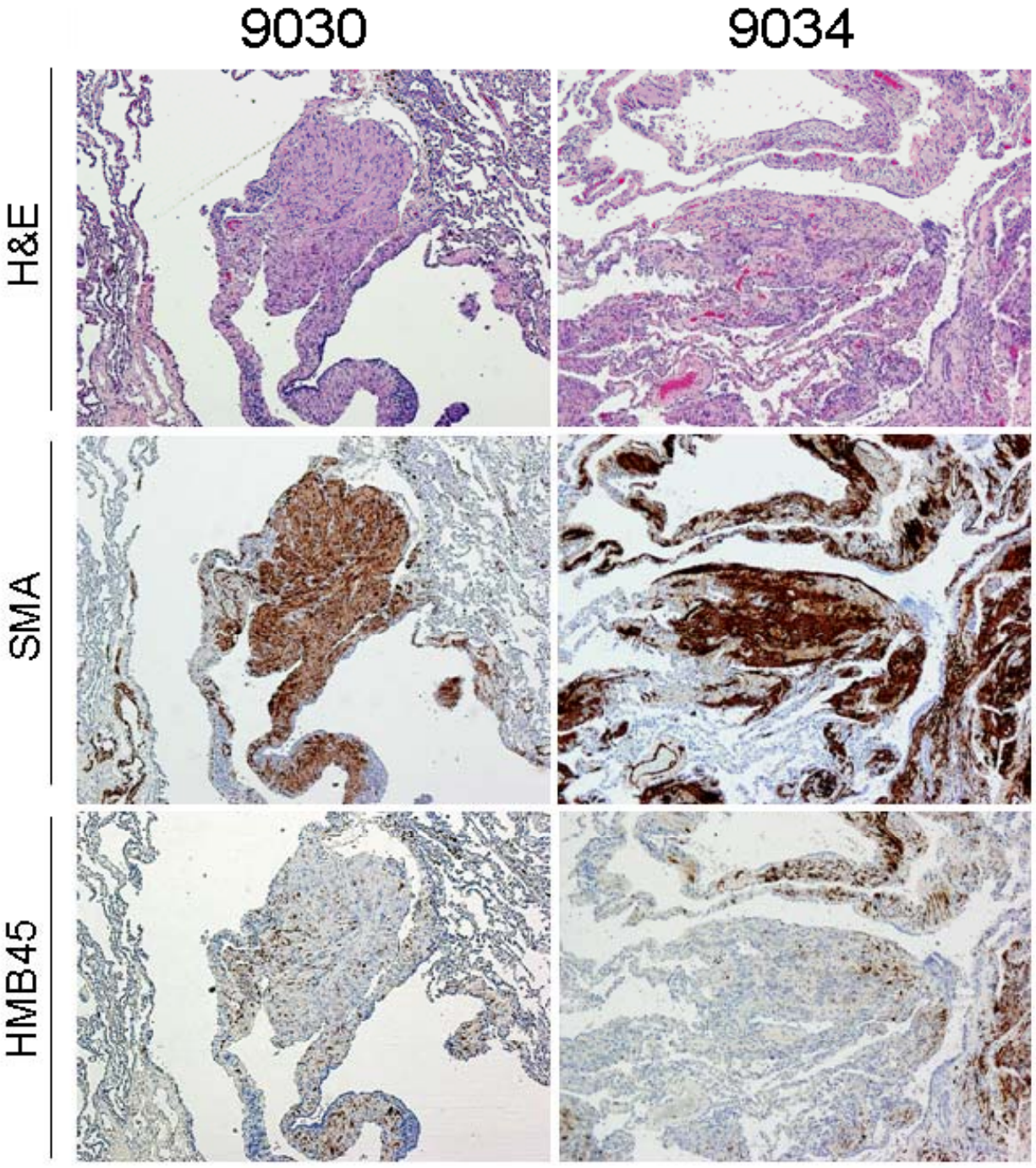

Supplemental Figure E8D

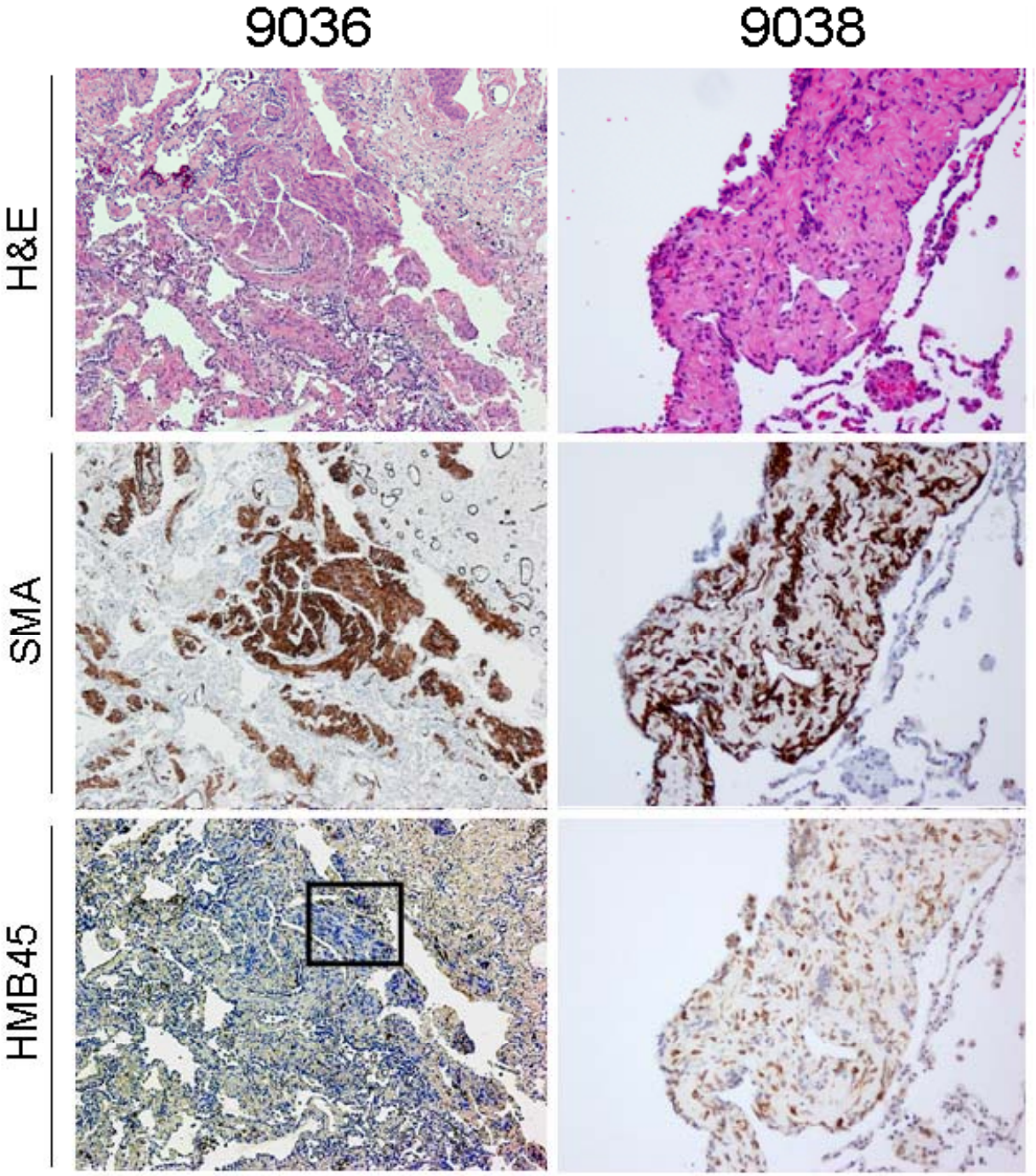

Supplemental Figure E8E

9036
inset

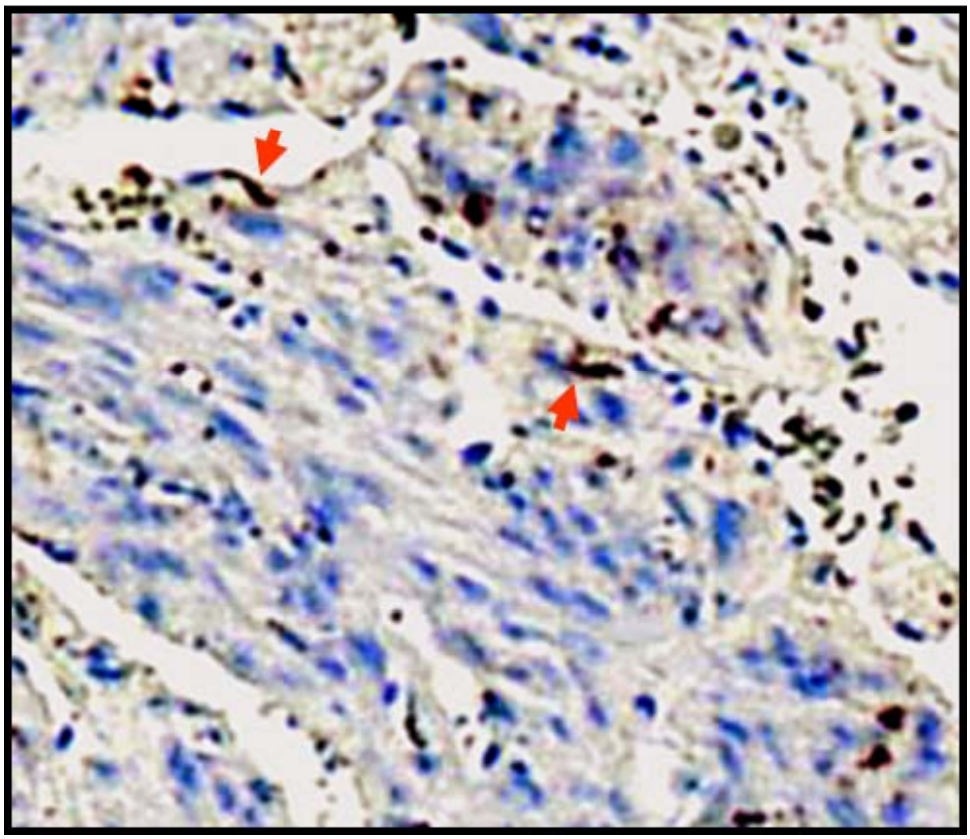

Supplemental Figure E8F

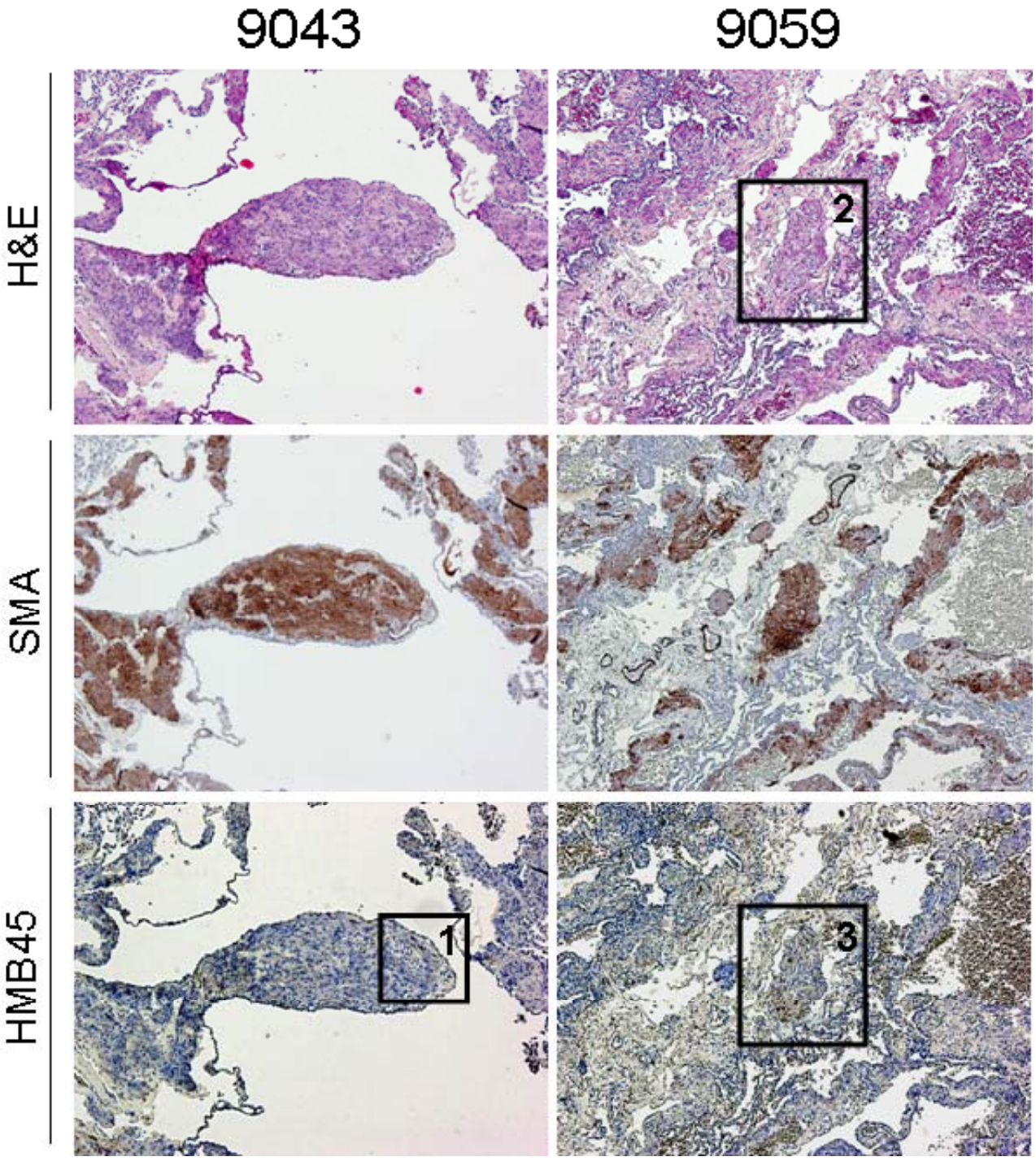

Supplemental Figure E8G

9043
inset

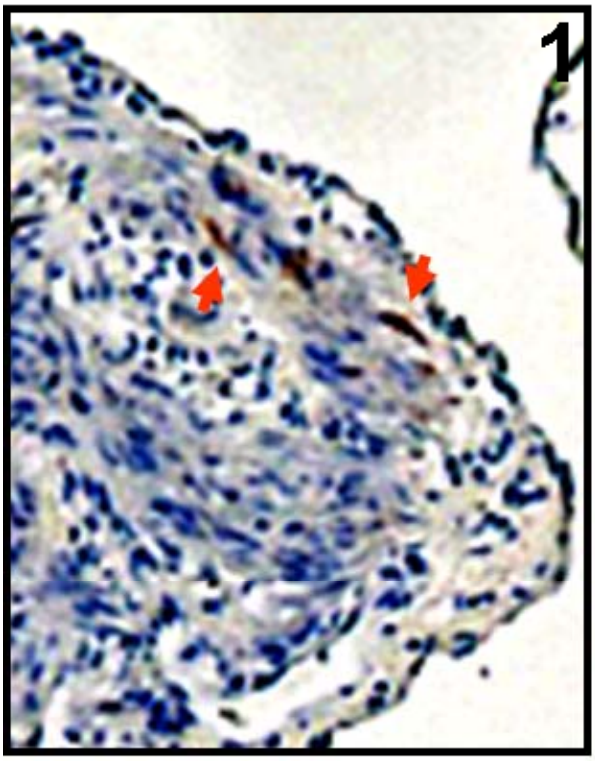

9059
insets

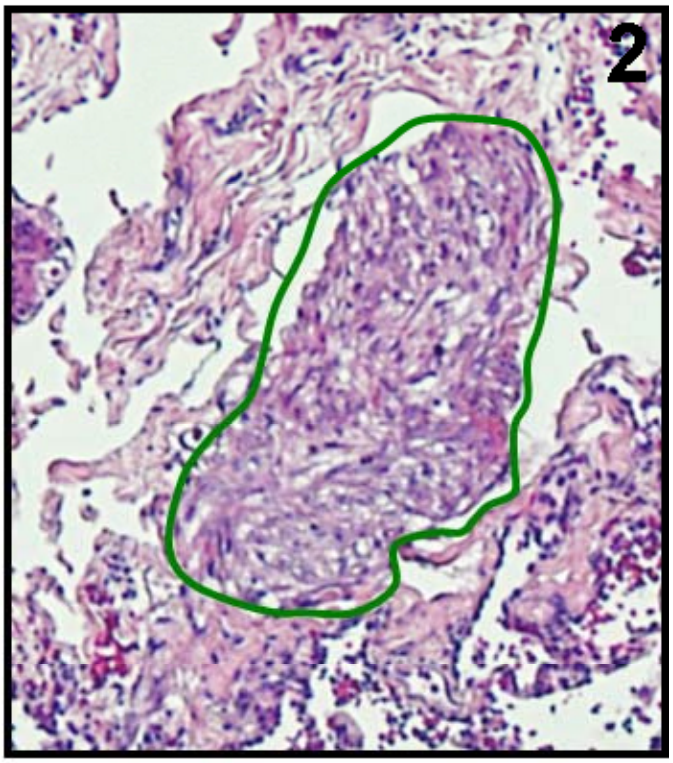

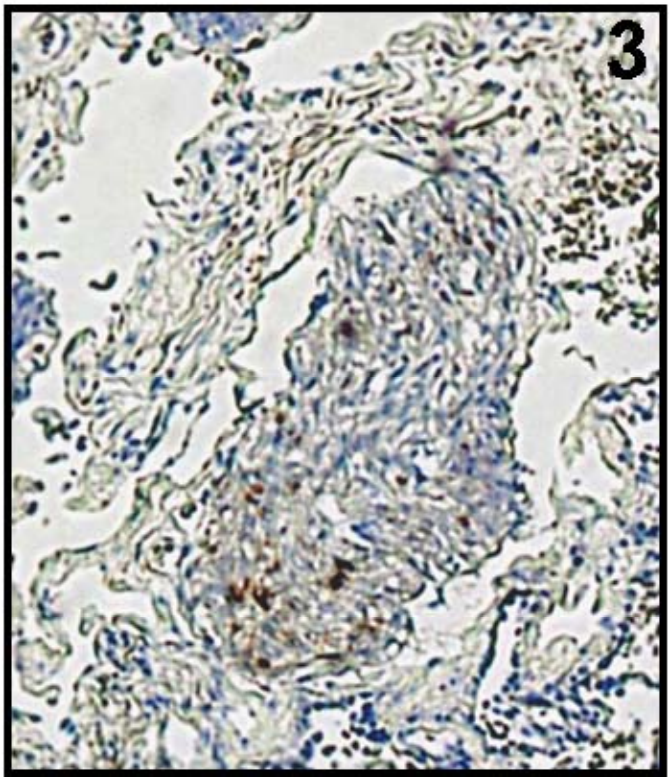

Supplemental Figure E9

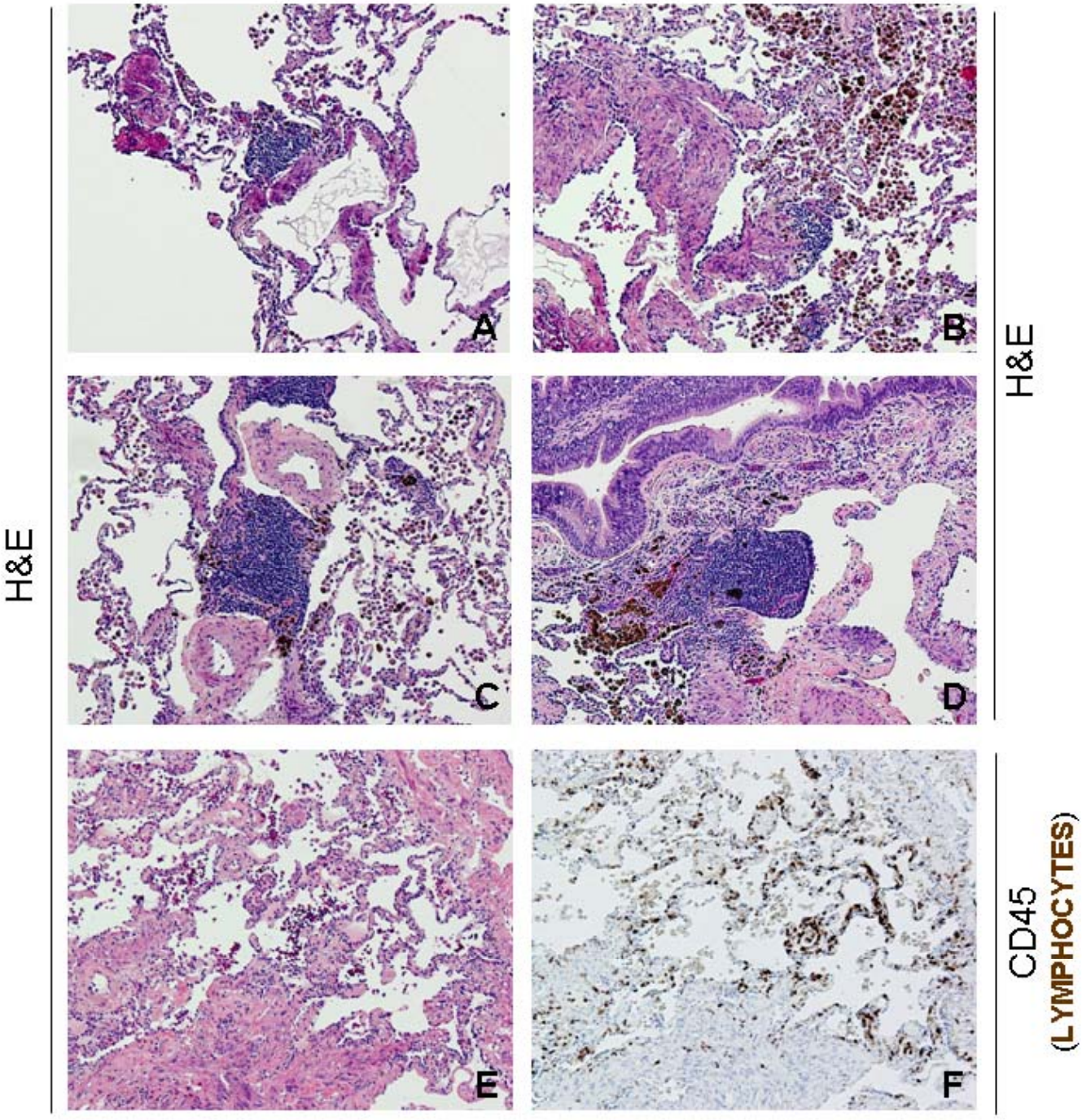

Supplemental Figure E10